Lasers in Manufacturing Conference 2019

Numerical Analysis of the Local Solidification Conditions in Laser Beam Welding of Aluminum Alloys

Jonas Wagner[a*], Christian Hagenlocher[a], Florian Fetzer[a], Constantin Böhm[b], Rudolf Weber[a], Stefan Weihe[b], Thomas Graf[a]

[a]*Institut für Strahlwerkzeuge (IFSW), Universität Stuttgart, Pfaffenwaldring 43, 70569 Stuttgart, Germany*
[b]*Materialprüfungsanstalt Universität Stuttgart, Pfaffenwaldring 32, 70569 Stuttgart, Germany*

Abstract

The local solidification conditions in full penetration laser welding of the aluminum alloy AA6016 were calculated. Therefore, a tailored numerical model was developed. Two sets of parameters with a large difference in absorbed line energy per welded depth were chosen in order to get an overview of the range of solidification parameters which is covered by full penetration welding. The results were applied to a solidification structure map in order to depict the implications on the local grain structure. Under consideration of the corresponding *y*-coordinates an estimation of the width of the equiaxed zone of the weld is possible.

Keywords: laser beam welding; grain structure; aluminum alloys; numerical modelling; welding simulation;

1. Introduction

In laser beam welding of aluminum alloys the resulting grain structure has an important influence on the strength of a weld seam as shown by Fujita and Tabata, 1973. This structure is strongly influenced by the local solidification conditions. In order to estimate the resulting grain structure solidification structure maps are used as shown for example by Kurz and Fisher, 1992.

A wide range of process parameters is used for laser beam welding with velocities between 0.25 m/min and 30 m/min, laser powers between 0.38 kW and 16 kW and beam diameters on the surface of the sample between 50 µm and 630 µm, as shown by Hagenlocher et al., 2019. The range in the structure maps resulting

* Corresponding author. Tel.: +49-711-685-66849; fax: +49-711-685-66842.
E-mail address: jonas.wagner@ifsw.uni-stuttgart.de.

from this variation of parameters is mostly indicated qualitatively, as shown for example by Dantzig and Rappaz, 2017. The present paper aims to give an overview over this range for welding of the aluminum alloy AA6016.

2. Numerical model

The numerical analysis to determine the local solidification conditions was performed based on the open source software *OpenFOAM*. A tailored numerical model was developed in order to achieve results on a short time scale with sufficient accuracy. The solidification conditions were derived from the temperature field, which was calculated numerically by solving the energy conservation equation using the finite volume method with consideration of the enthalpy of fusion, according to Rösler and Brüggemann, 2011. This has already been applied to laser beam welding by Fetzer et al., 2017. In the present paper only full penetration welding is considered. Therefore, two dimensional heat conduction was assumed.

A simplified capillary was implemented for the incoupling of the laser power. The geometry of the capillary was defined as a cylinder with a constant diameter corresponding to the diameter of the laser beam on the sample surface d_f. The heat, which is generated by absorbed laser energy, was taken into account as a boundary condition on the cylinder's surface as shown in Fetzer et al., 2017. The incoupling efficiency η and the evaporation temperature T_{evap} were set to a constant value at the beginning of the simulation. The incoupling efficiency η was estimated. A calculation of the intensity distribution on the modelled capillary through raytracing is planned as a further improvement of the simulation.

For pure aluminum the thermal conductivity is in the order of 200 W/(m K) at solid state, as shown by Kammer, 1998 and 100 W/(m K) at liquid state, as shown by Leitner et al., 2017. As shown for example by Mahin et al., 1991 the thermal conductivity for the liquid phase was increased to account for the convective heat transport through fluid flow which is not considered in the model. For the present paper the heat conductivity was approximated with the constant value of 200 W/(m K).

The solver proposed by Rösler and Brüggemann, 2011 was extended to allow for consideration of temperature dependent thermophysical properties. Properties within the solidification interval were calculated by the property of the solid-liquid mixture, as proposed by Ludwig, 2002.

The local solidification conditions are determined by the local temperature gradient and the solidification rate. The absolute value of the local temperature gradient

$$G = \|\nabla T\| = \sqrt{\left(\frac{\partial T}{\partial x}\right)^2 + \left(\frac{\partial T}{\partial y}\right)^2} \tag{1}$$

where T is the local temperature, x are the coordinates opposite to the feed direction and y are the coordinates transverse to the feed direction, can be derived from the calculated temperature field, according to Blecher et al., 2014. The z-direction is not considered because two dimensional heat conduction was calculated as explained above. Assuming that the direction of solidification is opposite to the direction of the temperature gradient the solidification rate

$$R = v \cdot \frac{1}{G} \cdot \left(-\frac{\partial T}{\partial x}\right) \tag{2}$$

where v is the feed rate opposite to the x direction, can be calculated as shown by Blecher et al., 2014.

3. Thermophysical properties

The constant parameters which were used to calculate the temperature field for laser beam welding of the aluminum alloy AA6016 are given in Table 1.

Table 1. Constant properties used in the simulation of full penetration welding of the aluminum alloy AA6016. [A]Calculated according to Andersson et al., 2002 with the software *Thermo-Calc 2018a TCAL5 Al-Alloys database version 5.1.* [B]Estimated from Kammer, 1998.

Parameter	Unit	Value
Incoupling efficiency η	-	0.83
Thermal conductivity λ_{th}	W/(m·K)	200
Enthalpy of fusion Δh_{f}	kJ/kg	403.175[A]
Evaporation temperature T_{evap}	K	2700[B]
Solidification interval $\Delta T = T_{liq} - T_{sol}$	K	925 – 861 = 63[A]

The used temperature dependent properties are shown in Fig. 1 (a). The values were calculated with the software *Thermo-Calc 2018a TCAL5 Al-Alloys database version 5.1* as shown by *Andersson et al., 2002*. A simplified chemical composition of AA6016 was used Al 98.52 wt.-%, Si 1.07 wt.-% and Mg 0.41 wt.-% for all *Thermo-Calc* calculations.

Fig. 1 (a) shows the integrated enthalpy of fusion and the solid fraction calculated by the Scheil solidification module of *Thermo-Calc*. Pre-set parameters for the Scheil solidification were used with a numerical

temperature step of 1 K. Fig. 1 (b) shows the values of the heat capacity and density as a function of the temperature. The heat capacity, density as well as the liquidus and solidus temperature were calculated with the equilibrium calculator of *Thermo-Calc* with pre-set parameters. The heat capacity and the density are approximated as constant above the maximum temperature shown in Fig. 1 (b) and are set to their value at *T* = 1500 K.

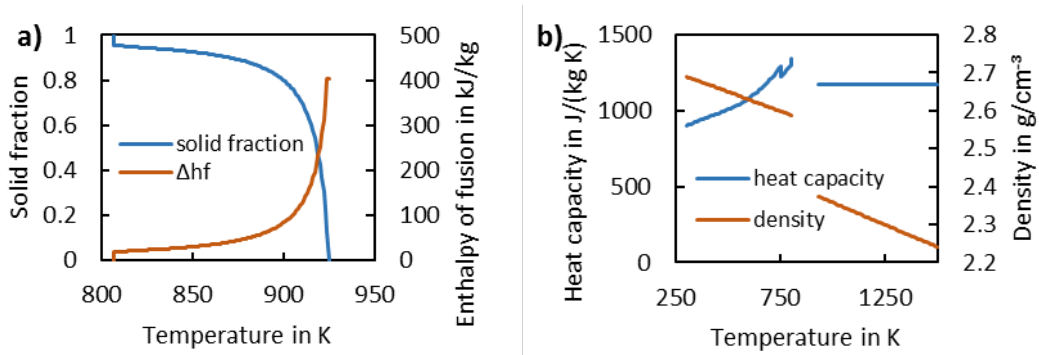

Fig. 1. Temperature dependent properties calculated with *Thermo-Calc 2018a TCAL5 Al-Alloys database version 5.1*, as shown in Andersson et al., 2002. (a) Temperature dependent solid fraction f_s and integral of enthalpy of fusion. (b) Calculated temperature dependent values of heat capacity and density.

An example for a simulated temperature field is depicted in Fig. 2. The simulated temperature was in the range of 293 K to 2400 K and is shown by the corresponding color, as indicated by the scale bar. The weld direction was from the left to the right. The simplified capillary, as explained above, is highlighted. The origin of the coordinate system in the center of the capillary, y transverse to the feed direction and x oppsite to the

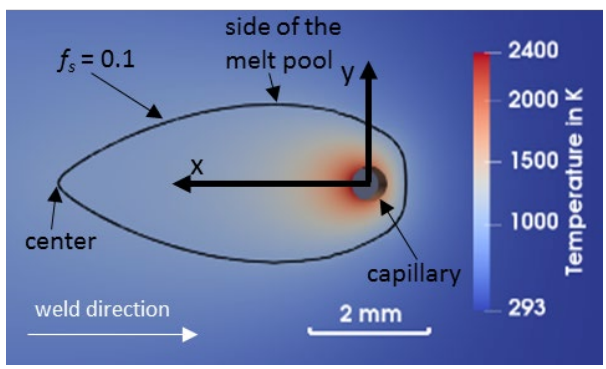

Fig. 2. Resulting temperature field for a simulation of the aluminum alloy AA6016 with P = 3.3 kW, v = 3 m/min, s = 2.4 mm, d_f = 600 µm, η = 0.83. The black line indicates the contour with f_s = 0.9.

feed direction are shown. The solidification conditions were evaluated at a solid fraction f_s of 0.1.The resulting contour is indicated by a black line in Fig. 2. The solidification takes place between the maximum *x*-coordinate at the center of the weld, highlighted as center and the maximum *y*-coordinate at the boundary of the melt pool, marked as side of the melt pool.

4. Calculation of the local solidification conditions

A large variety of process parameters is used for laser beam welding of aluminum with velocities between 0.25 m/min and 30 m/min, laser powers between 0.38 kW and 16 kW and beam diameters on the surface of the sample between 50 µm and 630 µm, as shown by Hagenlocher et al., 2019.

The absorbed line energy per welded depth

$$E_{depth} = \frac{P \cdot \eta}{v \cdot s} \quad (3)$$

where P is the laser power and s is the thickness of the sample, is a suitable key value to distinguish between the solidification conditions resulting from these different process parameters, as shown by Hagenlocher et al., 2019. Two distinct parameter sets with different E_{depth} were chosen, one with a low E_{depth} of 5.53 J/(mm²) and one with a high E_{depth} of 22.83 J/(mm²). This ensures that a large range of solidification conditions, which occur in actual full penetration laser welding processes of AA6016, is covered. These parameters and the resulting E_{depth}, calculated with an assumed incoupling efficiency of 83 %, are listed in Table 2.

Table 2. Process parameter sets used for the simulation.

Parameter	Unit	low-E_{depth}	high-E_{depth}
Laser power P	kW	0.8	3.3
Feed rate v	m/min	6	3
Beam diameter on sample surface d_f	µm	100	600
Thickness of sample s	mm	1.2	2.4
Absorbed line energy per welded depth E_{depth}	J/(mm²)	5.53	22.83

In Fig. 3 the numerically calculated values of G and R for the two parameter sets low-E_{depth} and high-E_{depth} are shown. R and G are depicted on the lower and upper horizontal axis, respectively and the corresponding y-coordinates are applied on the vertical axis. The red lines describe the calculated values of the temperature gradient and the blue ones describe the solidification rates.

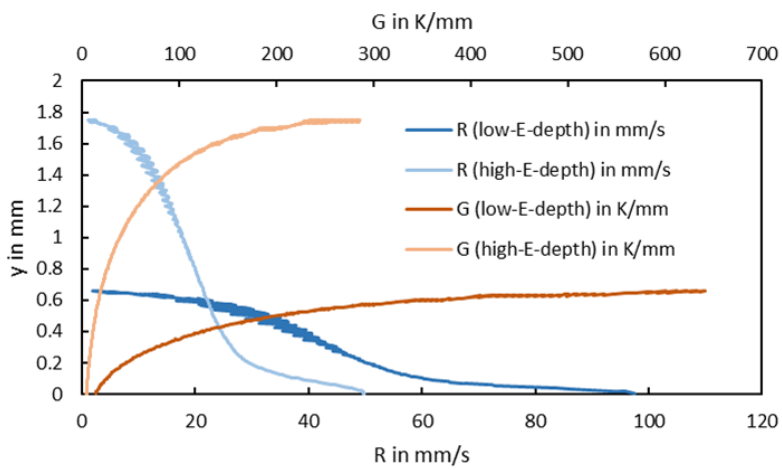

Fig. 3. Numerically calculated values of the temperature gradient G and the solidification rate R at the respective y-coordinates for f_s = 0.9. With P = 0.8 kW, v = 6 m/min, d_f = 100 µm, s = 1.2 mm (low-E_{depth}) and P = 3.3 kW, v = 3 m/min, d_f = 600 µm, s = 2.4 mm (high-E_{depth}).

It can be seen in Fig 3. that the parameter set low-E_{depth} results in a smaller weld pool with a maximum width $y_{max} \approx 0.7$ mm and high-E_{depth} results in a wider welt pool with $y_{max} \approx 1.8$ mm. At both parameter sets the gradient at the centerline (i.e. $y = 0$) is low with values below 20 K/mm and the solidification rate

approaches zero for y_{max}. The maximum values of *G* and *R* resulting from the low-E_{depth} are approximately twice the value resulting from the high-E_{depth}. This indicates the different local solidification conditions of both parameter sets. The results show that for laser beam welding of the alloy AA6016 minimal temperature gradients at the center of the weld pool of approximately 20 K/mm and maximum temperature gradients at the edge of the weld pool between 300 K/mm and 650 K/mm can be expected. The range of the calculated maximum of the solidification rate at the center of the weld pool lies between 50 mm/s and 100 mm/s.

5. Predicted grain structure

The different local solidification conditions have implications on the local grain structure. The calculated local solidification conditions (shown in Fig. 3) were transferred to the solidification structure map according to Kurz and Fisher, 1992, shown in Fig. 4. The horizontal axis describes the temperature gradient *G* and the vertical axis describes the solidification rate *R*. The blue line represents the transition from an equiaxed dendritic grain structure (above) to an oriented dendritic grain structure (below). The red line marks the transition from an oriented dendritic (above) to a non-dendritic cell structure (below). Indicated as grey lines are solidification conditions with the constant cooling rate

$$\dot{T} = \frac{\mathrm{d}T}{\mathrm{d}t} = G \cdot R \tag{4}$$

where t is the time. The purple line shows the solidification conditions for low-E_{depth}, the ones from high-E_{depth} are green. The values at the centerline and at the side of the melt pool as shown in Fig 2 are

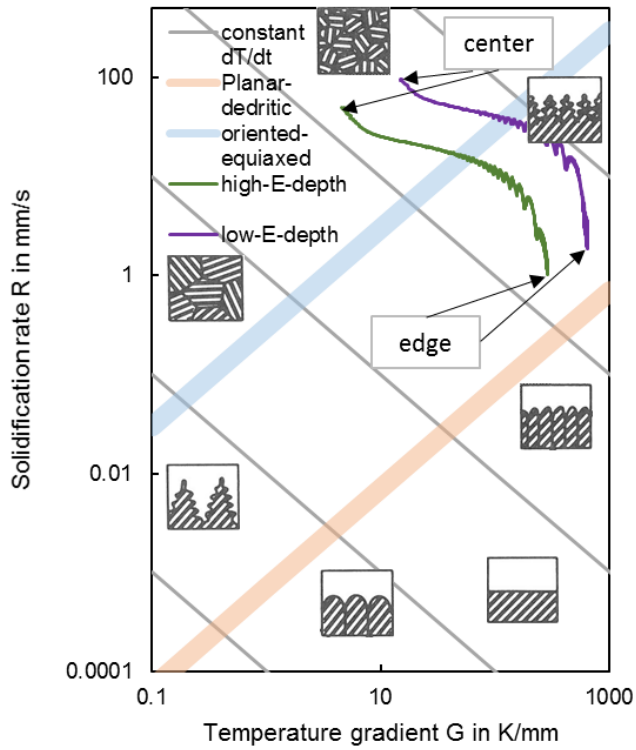

Fig. 4. Solidification structure map according to Kurz and Fisher, 1992 with the simulated results. With P = 0.8 kW, v = 6 m/min, d_f = 100 µm, s = 1.2 mm (low-E_{depth}) and P = 3.3 kW, v = 3 m/min, d_f = 600 µm, s = 2.4 mm (high-E_{depth}). Valid for a solidification interval $\Delta T \approx 50$ K.

highlighted.

Both curves in the solidification structure map exhibit a similar course, shifted by the cooling rate. This validates the direct influence of E_{depth} on the solidification conditions. According to Kurz and Fisher, 1992 the grain structure gets finer with increasing cooling rate. It can be concluded that with decreasing E_{depth} the grain structure gets finer, which was also shown by Hagenlocher et al., 2019. Moreover, it can be seen from the structure map that in both cases only dendritic structure is predicted.

Due to the choice of a low-E_{depth} and a high E_{depth} it can be assumed that the solidification conditions lie within the calculated range of G and R for most full penetration laser beam welding processes of the aluminum alloy AA6016, as shown by Hagenlocher et al., 2019. Therefore, it can be further assumed that the area between the two curves indicates the range of the solidification conditions and the range of the resulting grain structures.

The variation of G and R along y, as shown in Fig. 3, leads to an area of equiaxed grains. In both welds this area of equiaxed grains is predicted in the center of the weld seam.

6. Summary

A tailored numerical model based on *OpenFOAM* was developed which allows to calculate the local solidification conditions in full penetration welding. This model was used to determine the range of solidifications rates and temperature gradients which can be expected in full penetration welding processes of the aluminum alloy AA6016. Two sets of parameters were chosen with a large difference in E_{depth} to account for the variety of process parameters. The results show that for laser beam welding of AA6016 minimal temperature gradients at the center of the weld pool of approximately 20 K/mm and maximum gradients at the edge of the weld pool between 300 K/mm and 650 K/mm can be expected. The range of the calculated maximum of the solidification rate at the center of the weld pool lies between 50 mm/s and 100 mm/s. The solidification conditions were evaluated with the structure map from Kurz and Fisher, 1992 which gives an overview of the expected range of solidification parameters and allows for a prediction of the resulting grain structure. In both cases a dendritic structure is predicted with an equiaxed dendritic structure at the centerline of the weld seam and an oriented dendritic structure at the side.

7. Acknowledgement

This work was funded by the Deutsche Forschungsgemeinschaft (DFG, German Research Foundation) – 398552773.

References

Andersson J.-O., Helander T., Höglund L., Shi P., Sundman B., 2002. Thermo-Calc & DICTRA, computational tools for materials science. Calphad 26, pp 273–312. doi: 10.1016/S0364-5916(02)00037-8

Blecher J. J., Palmer T. A., DebRoy T., 2014. Solidification Map of a Nickel-Base Alloy. MTA 45, pp 2142–2151. doi: 10.1007/s11661-013-2149-1

Dantzig J. A., Rappaz M. (2017). Solidification, 2nd Edition. CRC PRESS, Boca Raton, Fl

Fetzer F., Stritt P., Berger P., Weber R., Graf T., 2017. Fast numerical method to predict the depth of laser welding. Journal of Laser Applications 29, p 22012. doi: 10.2351/1.4983152

Fujita H., Tabata T., 1973. The effect of grain size and deformation sub-structure on mechanical properties of polycrystalline aluminum. Acta Metallurgica 21, pp 355–365. doi: 10.1016/0001-6160(73)90191-0

Hagenlocher C., Fetzer F., Weller D., Weber R., Graf T., 2019. Explicit analytical expressions for the influence of welding parameters on the grain structure of laser beam welds in aluminium alloys. Materials & Design, p 107791. doi: 10.1016/j.matdes.2019.107791

Kammer C. (1998). Aluminium-Taschenbuch, 15. Auflage, 1. überarbeitete Ausgabe. Aluminium-Verlag, Düsseldorf

Kurz W., Fisher D. J. (1992). Fundamentals of solidification, 3. rev. ed. 1989, reprint. Trans Tech Publ, Uetikon-Zuerich

Leitner M., Leitner T., Schmon A., Aziz K., Pottlacher G., 2017. Thermophysical Properties of Liquid Aluminum. MTA 48, pp 3036–3045. doi: 10.1007/s11661-017-4053-6

Ludwig A., 2002. Thermophysical Properties Necessary for Advanced Casting Simulations. International Journal of Thermophysics 23, pp 1131–1146. doi: 10.1023/A:1019827900959

Mahin K. W., Winters W., Holden T. M., Hosbons R. R., MacEwen, 1991. Prediction and measurement of residual elastic strain distributions in gas tungsten arc welds. Welding Journal 70, 245s - 260s

Rösler F., Brüggemann D., 2011. Shell-and-tube type latent heat thermal energy storage: numerical analysis and comparison with experiments. Heat Mass Transfer 47, pp 1027–1033. doi: 10.1007/s00231-011-0866-9